RSC Advances

PAPER

View Article Online
View Journal | View Issue

Cite this: *RSC Adv.*, 2024, **14**, 32031

Synthesis and characterization of non-ionic flame-retardant waterborne polyurethane

Hongping Tong,[a] Weimin Wang,[c] Gui Wang,[a] Xiaojun Wang,[b] Dongmei Yu,[b] Bajin Chen[b] and Kemei Pei*[a]

Waterborne polyurethane (WPU) offers many advantages and is widely used in coatings, leathers, adhesives, biomaterials, and other consumer products. However, WPU is highly flammable. Many reactive flame retardants have been developed, but their char formation efficiency is still unsatisfactory, and the melt dripping during combustion has not been effectively suppressed. In this paper, a novel phosphorus-containing flame retardant with dihydroxy groups, (6-((4-hydroxyphenyl)((4-hydroxyphenyl)amino) methyl) dibenzo[c,e][1,2]oxaphosphinine 6-oxide) (PHAD), was successfully synthesized and incorporated into WPU molecular chain as a chain extender, thereby synthesizing a series of non-ionic flame-retardant waterborne polyurethane (NFRWPU) emulsions. The chemical structure of NFRWPU was successfully characterized by Fourier transform infrared spectroscopy and nuclear magnetic resonance. With the help of a thermogravimetric analyzer, scanning electron microscope and other instruments, some key performance parameters of NFRWPU in applications were investigated, including: physical, mechanical, and thermal stability and flammability. Some important experimental results include: both the particle size and viscosity of the emulsion increase gradually with increasing PHAD content, and when the PHAD content reaches 12%, the average particle size of emulsion increases to 106.6 nm with a viscosity of 89 mPa s; with the addition of PHAD, the tensile strength of NFRWPU initially increased and then decreased, while the elongation at break showed a continuous downward trend. The maximum tensile strength reached 22.63 MPa, and the minimum elongation at break dropped to 1060%; the addition of PHAD improved the thermal stability and flame retardancy of the film, with the highest limiting oxygen index value reaching 25.6% and the maximum carbon residue increasing to 6.5%. All these results indicate that NFRWPU is a promising flame retardant WPU considering the comprehensive performance.

Received 13th August 2024
Accepted 6th October 2024

DOI: 10.1039/d4ra05873a

rsc.li/rsc-advances

Introduction

Waterborne polyurethane (WPU) offers advantages such as being environmentally friendly, nontoxic, abrasion resistant, and low-temperature flexible, and is widely used in coatings, leathers, adhesives, biomaterials, and other consumer products.[1,2] However, WPU is highly flammable (the limiting oxygen index of ordinary WPU materials is only ~18%).[3] During combustion, the toxic gases produced can lead to severe melt dripping and rapid fire spread,[4] which may cause suffocation or even death of affected individuals. Therefore, extensive research efforts are focused on flame-retardant modification of WPUs to improve their fire safety in applications.

Although halogenated flame retardants can improve flame retardancy, they are harmful to the environment and release toxic gases such as hydrogen halide during combustion.[5] With increasing environmental awareness, more and more halogen-free flame retardants have been developed, mainly including additive and reactive flame retardants.[6] For additive flame retardants, such as montmorillonite, expandable graphite, aluminum hypophosphite, triethyl phosphate, *etc.*,[7] these additives have poor compatibility with the matrix, which may deteriorate mechanical and thermal insulation properties of WPU.[8] Reactive flame retardants are introduced during the synthesis of PU and become part of PU molecular structure by participating in chemical reactions with other starting materials,[9] achieving permanent flame retardancy.[10] So far, many reactive flame retardants have been reported for synthesizing WPU. Reactive flame retardants containing P, Si and N groups have been shown to form chemical bonds with main/side chains of the polymer matrix while basically maintaining physical and mechanical properties of WPU and excellent flame retardancy.[11] For example, the flame retardant mechanism of

[a]*School of Chemistry and Chemical Engineering, Zhejiang Sci-Tech University, Hangzhou 310018, China. E-mail: peikemei@zstu.edu.cn*

[b]*Hangzhou Transfar Fine Chemical Co., Ltd, Hangzhou 311215, China*

[c]*School of Materials Science and Chemical Engineering, Ningbo University, Ningbo, 315211, China*

phosphorus-containing flame retardants (PFRs) involves the generation of phosphoric acid and polyphosphoric acid during combustion, which can cause dehydration and catalyzing formation of carbonization layer in condensed phase, or form active radicals to scavenge reactive radicals in gas phase,[12,13] thereby delaying polymer chains decomposition and blocks internal heat release and flame transfer.[7,14] Although these systems have achieved many valuable results, the char formation efficiency is still unsatisfactory, and the melt dripping of corresponding WPU during combustion has been not effectively suppressed.[6]

Among various PFRs, 9,10-dihydro-9-oxo-10-phosphaphenanthrene-10-oxide (DOPO) and its derivatives have attracted much attention due to their high thermal stability, excellent flame retardancy, and low toxicity owing to presence of cyclic phosphate groups with a diphenyl structure (phosphophenanthrene structure).[7,15] DOPO and its derivatives can undergo reactions through P–H bond of DOPO with double bond –C=C– and –C=N– of substrates.[16] Compared with other linear low-molecular-weight phosphorous compounds, DOPO have higher char formation efficiency and anti-dripping effect.[17] Zhou *et al.* synthesized a DOPO-based aromatic Schiff base derivative, and successfully incorporated it into the main chain structure of WPU. This modification increased the LOI value to 27.9%.[6] Liang *et al.* used dangling polydimethylsiloxane and a DOPO-derived phosphoamide diphenol as chain extenders and incorporated them into the main chain of WPU, improving the thermal stability and flame retardancy.[16] Ren *et al.* also developed a novel flame-retardant polyurethane acrylate based on DOPO. Unfortunately, the rigid heterocyclic structure of DOPO decreases the segment flexibility of WPU.[18] In conclusion, DOPO-derived synthesized WPU is still in early stage, and it is difficult to balance the anti-dripping during combustion with DOPO dosage, because the improvement of WPU's flame retardancy often comes at the expense of its unique mechanical properties,[6] thereby requiring experiments to regulate and optimize proportion of flame retardants.

Most WPUs developed today stabilize the WPU by introducing nonionic and/or ionic hydrophilic groups into the polymer chain.[19] Based on these hydrophilic groups, WPUs can be classified as anionic (*e.g.*, dimethylolpropionic acid and sulfonates), cationic (*e.g.*, *N*-methyl diethanolamine (MDEA)), or nonionic. Nonionic WPUs rely primarily on the hydrophilicity of polyethylene glycol chain segments (–CH_2–CH_2–O–) introduced into the main or side chains to achieve PU dispersion in water.[20] Since there is no double electric layer structure as in ionic PU emulsions,[21] nonionic WPU emulsions are insensitive to electrolytes and pH, and thus have good biocompatibility and excellent acid and alkali resistance and electrolyte stability.[22] Nevertheless, nonionic flame retardants have not been reported.

In this paper, a novel phosphorus-containing flame retardant with dihydroxy groups, (6-((4-hydroxyphenyl)((4-hydroxyphenyl)amino)methyl)dibenzo[*c*,*e*][1,2]oxaphosphinine 6-oxide) (PHAD), was successfully synthesized and incorporated into WPU molecular chain as a chain extender, thereby synthesizing a series of non-ionic flame-retardant waterborne polyurethane (NFRWPU) emulsion. PHAD replaces the traditional small molecule chain extender[23] and serves as a monomer in NFRWPU, which introduces the phosphorus element in PHAD into the molecular chain of WPU through chemical reactions, thus imparting flame retardancy to the material. The chemical structure of NFRWPU was successfully characterized by Fourier transform infrared spectroscopy and nuclear magnetic resonance. With the help of thermogravimetric analyzer, scanning electron microscopy and other instruments, some key performance of NFRWPU in applications were investigated, including: physical, mechanical, thermal stability and flammability.

Experiment

Materials

p-Hydroxybenzaldehyde, *p*-aminophenol, polyethylene glycol 2000 (PEG2000), polyether polyol (N210), trimethylolpropane (TMP) and DOPO were purchased from Shanghai Macklin Biochemical Co., Ltd (analytical-grade, Shanghai, China). Toluene diisocyanate (TDI) was purchased from Shandong Jiaying Chemical Technology Co., Ltd (industrial grade, Jinan, China). Ethylenediamine (EDA) was purchased from Shanghai Lingfeng Chemical Reagent Co., Ltd (analytical grade, Shanghai, China). Anhydrous ethanol, acetone, acetic acid and toluene were supplied by Hangzhou Shuanglin Chemical Reagent Co., Ltd (analytical grade, Hangzhou, China). 4 A molecular sieves were purchased from Sinopharm Chemical Reagent Co., Ltd (Shanghai, China).

Synthesis of PHAD

The entire reaction process for phosphorus-containing flame-retardant monomer PHAD was shown in Scheme 1. First step is to synthesis 4-((4-hydroxybenzylidene) amino) phenol (PHA). *p*-Aminophenol (18 g, 0.15 mol), *p*-hydroxybenzaldehyde (18.32 g, 0.15 mol), acetic acid (0.45 g, 0.0075 mol), 4 A molecular sieves (8 g), and 360 mL ethanol were added into a 500 mL four-neck flask (nitrogen inlet, condenser, thermometer, and mechanical stirrer), which was placed into a 70 °C water bath for 8 h. Then, pour the reaction mixture into a prepared ice-water bath, where a large amount of orange solid will precipitate. Filter the solid under vacuum and wash it twice with deionized water. The solid was dried in a vacuum oven at 100 °C to a constant weight to give an orange-yellow PHA powder (88.46% yield). The second step is to synthesis PHAD. Place DOPO (17.30 g, 0.08 mol), PHA (17.04 g, 0.08 mol), and 300 mL ethanol into a 500 mL four-neck flask. Conduct the reaction in an ice-water bath, maintaining the reaction temperature at 3–5 °C for 6 h. Then, pour the reaction mixture into a prepared ice-water bath, where a large amount of pale-yellow solid will precipitate. Filter the solid under vacuum and wash it twice with deionized water. The solid was dried in a vacuum oven at 100 °C to constant weight to give pale-yellow PHAD powder (90.13% yield). ^{1}H-NMR (400 MHz, $CDCl_3$): d = 7.0–8.2 (8Ar–H_{6-13}), 6.3–7.2 (8Ar–H_{2-5}), 5.5–6.1 (NH and NH′), 4.7–5.3 (P–C–H_1, P–C–$H_{1'}$) (see Fig. 2b).

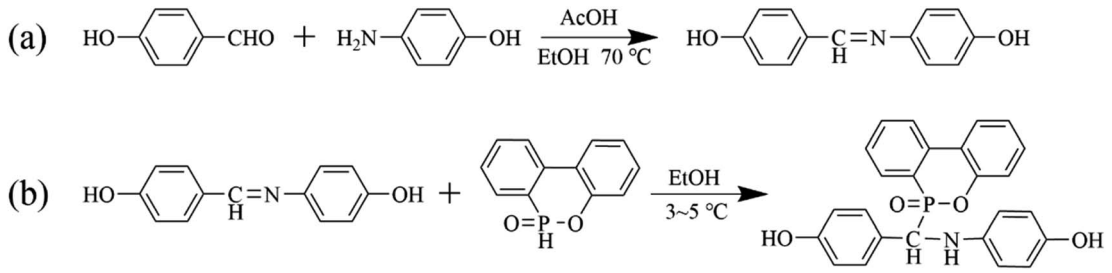

Scheme 1 Synthesis of (a) PHA and (b) PHAD monomer.

Synthesis of NFRWPU

NFRWPU emulsion synthesis principle is shown in Scheme 2. N210, PHAD and PEG2000 were dehydrated (120 °C, 0.1 MPa) under vacuum for 6 h, and then cooled to room temperature for use. The synthesis method of NFRWPU is as follows: firstly, TDI (29 g), N210 (56 g) and ethanol solvent (50 mL) were added to a nitrogen-protected four-necked flask, stirred at room temperature for 0.5 h, and heated up to 80 °C and reacted for 3 h; after the flask was cooled to 70 °C, crosslinker TMP (3.0 g), PHAD (15.0 g) and acetone solvent (20 mL) were added to the flask to perform extension reaction for 1 h; after the flask was cooled to 60 °C, hydrophilic chain extender PEG2000 (20 g) was added and reacted for 3 h; after cooled to 20 °C, post-chain extension EDA (2.0 g) and acetone (20 mL) were added and reacted for 1 h; finally, deionized water was added and emulsified with high-speed stirring for 1 h. The residual acetone was removed by distillation under reduced pressure to obtain NFRWPU.

Preparation of NFRWPU

The NFRWPU emulsions are poured uniformly into a PTFE mold and left to dry for one day in a natural environment. After the water has evaporated, the films were placed in a vacuum oven and dried at 120 °C for 20 minutes until the weight of films no longer changes. The dried films should be stored in a desiccator to ensure the purity of the films. Specifically, in this paper, according to the mass percentages of PHAD (%) in the NFRWPU, the synthetic NFRWPU emulsion is named as NFRWPU$_X$, where X takes values of 9, 12, 15, and 18%, respectively. The formulations of NFRWPU were shown in Table 1.

Characterization and measurements

Nuclear magnetic resonance (NMR) ^{1}H spectra were recorded using a Bruker Avance II DMX400 NMR spectrometer operating at 400 MHz at room temperature using $CDCl_3$ as the NMR solvent.

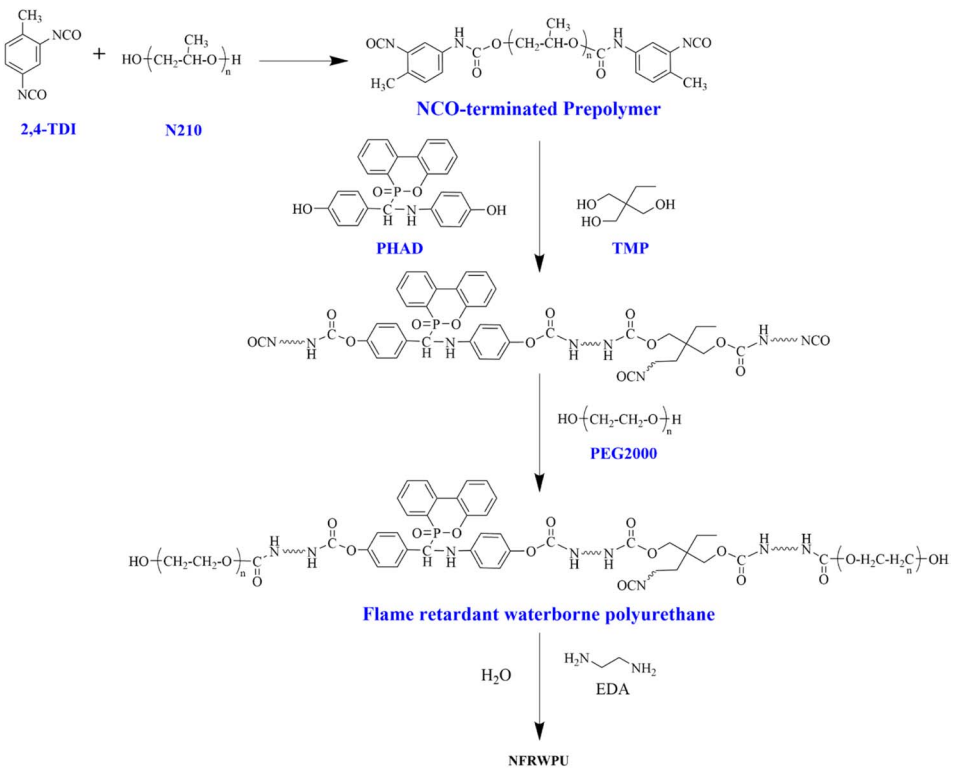

Scheme 2 Synthesis of NFRWPU emulsion.

Table 1 Formulations of NFRWPU containing different PHAD contents[a]

Sample	Component (g)					
	PHAD	TDI	PHAD	PEG2000	TMP	EDA
WPU	56.0	29.0	0.0	20.0	5.0	2.0
$NFRWPU_9$	56.0	29.0	11.0	20.0	4.0	2.0
$NFRWPU_{12}$	56.0	29.0	15.0	20.0	3.0	2.0
$NFRWPU_{15}$	56.0	29.0	19.6	20.0	2.0	2.0
$NFRWPU_{18}$	56.0	29.0	23.8	20.0	1.2	2.0

[a] $NFRWPU_x$, where the X denotes the mass percentages of PHAD; X = mass(PHAD)/m(N210 + TDI + PHAD + PEG2000 + EDA) × 100%.

Prepare NFRWPU emulsion as described above for film preparation. Utilize a Fourier Transform Infrared (FT-IR) spectrometer to characterize the sample in the range of 4000–650 cm^{-1} over 32 scans times at a resolution of 4 cm^{-1} on Nicolet 5700 FTIR spectrometer.

Thermogravimetric analysis was measured on a NETZSCH TG 209F1 thermogravimetric analyzer (TGA). The film prepared from the emulsion were taken and dried in a vacuum drying oven for 8 h. Samples weighing 1–5 mg were placed in the TGA and heated from 20 to 600 °C at a heating rate of 20 °C min^{-1} under a flow of nitrogen (50 mL min^{-1}).

Physical properties of NRWPU emulsions were tested including appearance, storage stability, viscosity and particle size. The storage stability test method on a 3K15 high-speed refrigerated centrifuge was as follows: the same amount of NFRWPU was placed in a centrifuge and centrifuged at 3000 rpm for 15 min. If there was no settlement, it could be considered that there was a storage stability period of 6 months.[24] The viscosity was obtained on a Thermo Haake RheoStress 300 rheometer at 25 °C. The particle size is tested using nanoparticle size analyzer, HORIBA SZ-100V2. Take 2–3 drops of emulsion in a cuvette and dilute it with deionized water to the scale value to test the particle size distribution.

The film mechanical properties, including tensile strength, elongation at break were determined by mechanical testing machine (RGT-20A, Shenzhen Reger Instrument Equipment Co., Ltd, China). All specimens (150 × 20 × 0.5 mm) were tested in quintuplicate and the average values were reported according to GB/T 1040.3-2006.

Flammability tests include Limiting Oxygen Index (LOI) test and a vertical burning test. The LOI was obtained according to the standard GB/T 2406.2-2009. The LOI refers to the minimum oxygen concentration at which a material can sustain combustion in a mixture of nitrogen and oxygen. An oxygen index instrument (JF-3, Dongguan Best Instrument Equipment Co., Ltd, Dongguan, China) was used on films (150 × 58 × 1 mm). The sample is vertically clamped in a sample holder on the combustion tube, ignited at the top in a flow of oxygen and nitrogen, and the burning process and related data are recorded.

The vertical burning test was according to GB/T 8626-2007 standard. Take a sample (150 × 58 × 1 mm) and vertically fix it on an iron stand. Place a piece of filter paper beneath the sample. Use the outer flame of a flame source to ignite the bottom edge of the sample for 5 seconds. Record the following observations: Whether the sample ignites and the time taken to ignite. Self-extinguishing time after removing from the flame. Whether burning material drips and ignites the filter paper.

Scanning electron microscopy (SEM) with energy-dispersive X-ray spectroscopy (EDS) experiments were performed using a Hitachi S-4800. The micromorphology of the residual char after combustion with a conductive gold layer was observed using low-temperature fracturing under high vacuum at a voltage of 15 kV.

Results and discussion

Characterization of PHAD

FT-IR spectroscopy. Fig. 1a shows FTIR spectra of PHA and PHAD, and it can be observed that PHA (black line) has an obvious peak at 1586 cm^{-1}, which is characteristic of stretching vibration of C=N, confirming formation of Schiff base structure from the condensation of aldehyde and amine. In contrast, PHAD (red line) shows characteristic peaks of DOPO structure around at 1202, 930, and 752 cm^{-1}, attributed to stretching vibrations of P=O, P–O–Ar, and P–C, respectively. Additionally, the spectrum of PHAD shows a new peak at 1370 cm^{-1} corresponding to stretching vibration of C–N, while the typical stretching vibration of C=N at 1651 cm^{-1} disappears, which further confirms the successful addition reaction of P–H in DOPO with C=N in PHA. In Fig. 1b, the FTIR spectra of WPU (black line) and $NFRWPU_{12}$ (red line) show classic absorption peaks of polyurethane structure. No absorption peaks of –NCO groups are observed in range of 2260–2280 cm^{-1}, indicating complete participation of –NCO in the reaction after polymerization and chain extension, with no unreacted –NCO present in WPU and $NFRWPU_{12}$. Furthermore, $NFRWPU_{12}$ exhibits characteristic peaks of PHAD around at 1410, 925 and 715 cm^{-1}, attributed to stretching vibrations of P–Ph, P–O–Ar and P–C, respectively. The appearance of these three characteristic peaks indicates that the synthesis of PHAD-modified flame-retardant WPU was successful. Since the absorption peaks of P=O group in PHAD and C–O–C bond in WPU both appeared around 1220 cm^{-1}, the presence of P=O group cannot be distinguished from the FTIR spectrum of $NFRWPU_{12}$.

NMR spectrometry. ^1H NMR spectra of PHA and PHAD (see Fig. 2). In Fig. 2a, PHA shows a singlet at 8.5 ppm (5), attributed to the proton of H–C=N, and multiplets from 6.7 to 7.8 ppm (1–4, 6–9), attributed to protons of benzene ring. These results are similar to those reported for a PHID by Cui *et al.*[25] After reacting DOPO with PHA, in Fig. 2b, PHAD shows characteristic phosphorus-phenyl protons in the range of 7.0–8.2 ppm (6–13).[26] Therefore, the multiplet for benzene ring protons (2, 3, 4, 5) shifts to 6.3–7.2 ppm due to different chemical environments, all proving that DOPO has successfully grafted onto PHA. Two secondary amine peaks (NH and NH′) appear at 5.5–6.1 ppm, and two aliphatic hydrogen peaks (1 and 1′) appear at 4.7–5.3 ppm due to the presence of two enantiomers, which was attributed to the proton of P–C–H.[27] These demonstrates the successful synthesis of PHAD.

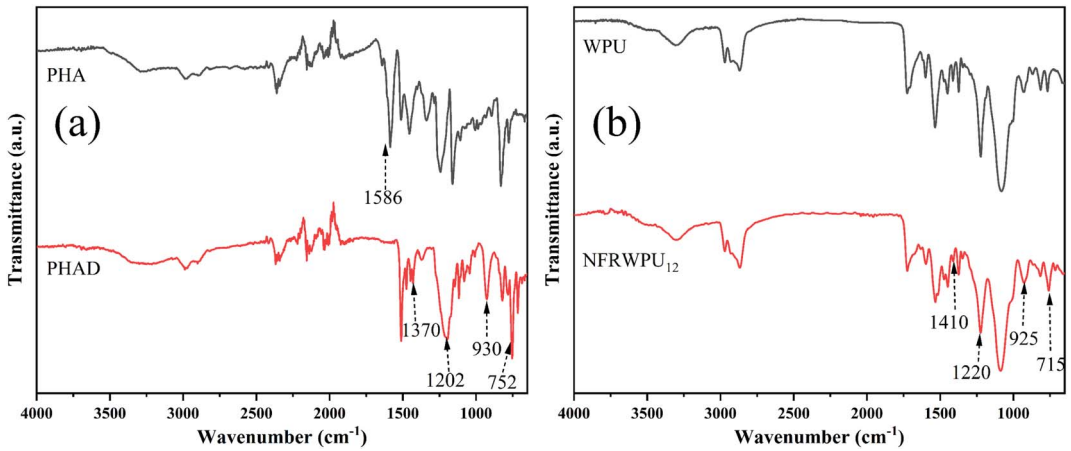

Fig. 1 FT-IR spectra of (a) PHA with PHAD and (b) WPU with $NFRWPU_{12}$.

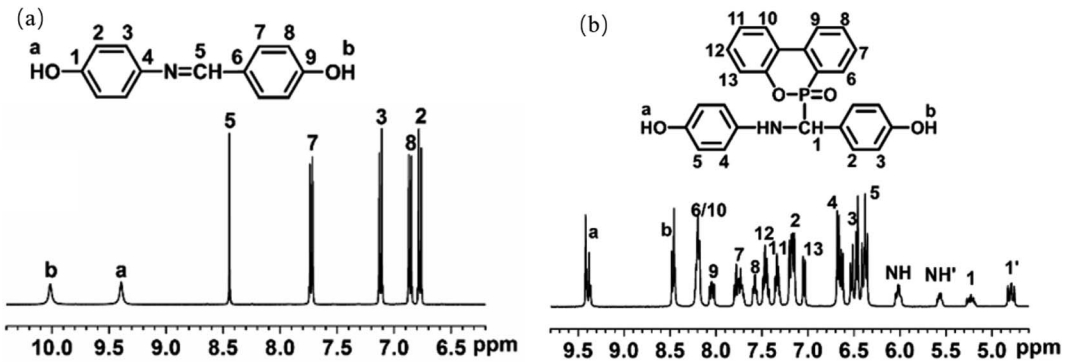

Fig. 2 ^{1}H NMR spectra of (a) PHA and (b) PHAD.

Physical properties of NFRWPU

In synthesis of NFRWPU, PHAD replaced traditional small molecule chain extender BDO as pre-chain extender.[23] Due to PHAD's higher molecular weight and molecular structure containing multiple rigid phenyl groups, its content significantly affects the physical properties of emulsion. As can be seen from Table 2, as PHAD content increases, the appearance of emulsion gradually changes from a Milky white with slight bluish tint to dark yellow, indicating that the particle size of WPU was the smallest. When PHAD content is <18%, the synthesized emulsions can pass stability test, indicating that they have excellent storage stability and storage life (>6 months). No precipitation appeared in the emulsions after centrifugation, indicating that the prepared dispersions were stable and could be stored stably for a long time. The emulsion viscosity also gradually increases with PHAD content. However, when PHAD content increases to 18%, the emulsion color becomes dark yellow, and the emulsion stability deteriorates. This may be due to the excessive molecular weight of prepolymer, resulting in too high viscosity of solution, and the emulsification process becomes difficult during post-chain extension, significantly reducing the stability of emulsion, making it unable to form a film.

The particle size distribution of NFRWPU with PHAD content was presented in Fig. 3 and the data are listed in Table 2. It can be seen that the particle size of NFRWPU without PHAD showed a unimodal distribution with an average particle size

Table 2 Effect of PHAD content on physical properties of NFRWPU emulsions

Sample	Emulsion appearance	Storage stability	Viscosity (mPa s)	Particle size (nm)
WPU	Milky white with slight bluish tint	No precipitation	67	49.3
$NFRWPU_9$	Light yellow opaque	No precipitation	75	103.1
$NFRWPU_{12}$	Light yellow opaque	No precipitation	89	106.6
$NFRWPU_{15}$	Milky yellow opaque	No precipitation	105	134.9
$NFRWPU_{18}$	Dark yellow	Precipitation	—	—

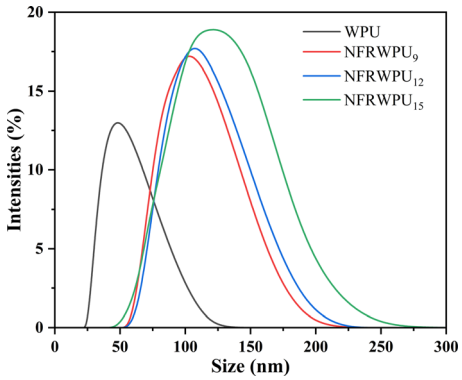

Fig. 3 Particle size distribution of NFRWPU with PHAD contents.

about 49.3 nm. The particle size of NFRWPU increased with the increase of the content of PHAD, and the particle size of NFRWPU increased from 103.1 nm to 134.9 nm. The reason may be that the increase of PHAD content led to the increase of steric hindrance from the phosphaphenanthrene structure, thus limiting molecular chain mobility, and consequently increased the particle size.[28]

Mechanical properties of NFRWPU

To investigate influence of PHAD content on mechanical properties of NFRWPU, tensile tests were conducted, and specific data are shown in Table 3. With the increase of PHAD content, the tensile strength of NFRWPU initially increases to a peak and then begins to decrease, while the elongation at break displayed a downward trend. When PHAD content increases from 0 to 12%, the tensile strength of the film significantly increases from 2.83 MPa to 22.63 MPa. However, further increasing the PHAD content results in a decrease in tensile strength. At 18% PHAD content, the emulsion stability was poor and the film formation was not good, therefore, the mechanical properties of the $NFRWPU_{18}$ film could not be evaluated. The elongation at break decreases from 1380% to 1060% with the increase of PHAD content. These results can be explained as follows: firstly, the phosphorus-containing rigid segments in PHAD molecular structure (aromatic rings) can enhance mechanical properties of the film.[25] Secondly, the P–H bonds in PHAD molecules are polar covalent bonds that can form hydrogen bonds with WPU molecular chains, enhancing intermolecular cohesion.[13] Consequently, with increasing PHAD content, the tensile strength of NFRWPU films also increases within a certain range. However, excessive PHAD can disrupt the hydrogen bonding in WPU, complicate emulsification process, and lead to a decrease in film's mechanical properties. The decrease in elongation at break is primarily due to steric hindrance effects caused by large rigid structure of PHAD, which restrict molecular chain mobility.[13] Additionally, excessive PHAD can reduce emulsion stability, impair film forming properties, and result in cracked or non-film-forming surfaces. Therefore, the optimal addition of PHAD is determined to be 12%.

Table 3 Effect of PHAD content on mechanical properties of NFRWPU film

Sample	Tensile strength (MPa)	Elongation at break (100%)
WPU	2.83	1380
$NFRWPU_9$	10.61	1320
$NFRWPU_{12}$	22.63	1220
$NFRWPU_{15}$	13.08	1060
$NFRWPU_{18}$	—	—

Thermal stability of NFRWPU

Based on above mechanical properties, $NFRWPU_{12}$ was selected for the study. Fig. 4 illustrates TGA and differential thermal gravity (DTG) curves of WPU and $NFRWPU_{12}$, respectively, and some data and definitions are recorded in Table 4. The DTG curves displayed two T_{max}, suggesting two-stage process for thermal degradation of NFRWPU and WPU: the first stage is around 340 °C, primarily attributed to decomposition of urethane bonds and carbamate groups, corresponding to hard segments degradation;[28] the second stage is around 400 °C, corresponding to decomposition of polyether segments, representing soft segments degradation.[28] The $T_{5\%}$ of WPU film is 301.72 °C, while the $T_{5\%}$ of $NFRWPU_{12}$ film drops to 283.63 °C, indicating first-stage thermal decomposition starts earlier, which attributes to the lower bond energy of the P–C bond (264 kJ mol^{-1}) compared to the C–C bond energy (331 kJ mol^{-1}), thus lowering thermal stability of the film. In Table 4, T_{max} and RT_{max} of $NFRWPU_{12}$ are also reduced compared with that of WPU, which is mainly because the phosphoric acid derivatives (phosphoric acid-like substances) produced by the decomposition of $NFRWPU_{12}$ can catalyze generated polyol to dehydrate and carbonize.[6] At 600 °C, the residual carbon of $NFRWPU_{12}$ reaches 6.55 wt%, which was about 7 times that of WPU. In summary, under the action of PHAD, the NFRWPU forms a protective carbon layer at lower temperatures, thereby suppressing mass loss at high temperatures. The formation of the carbon layer not only blocks heat transfer during combustion, but also isolates combustible gases, effectively inhibiting degradation of underlying polymer and increasing carbon residue.

Flammability of NFRWPU

The flammability of WPU and NFRWPUs were investigated by LOI and vertical burning tests. As shown in Table 5, pure WPU is a flammable material (LOI value of only 18.5%). However, by introducing flame retardant PHAD into polyurethane molecular chain, the LOI value of NFRWPU film increases. Specifically, when PHAD content increases from 0 to 12%, the LOI value of the film increases from 18.5% to 25.6%. This change is primarily attributed to the low bond energy of the P–C bond, which breaks at lower temperatures to produce phosphoric acid, polyphosphoric acid, and their derivatives. These products act as catalysts to promote polymer dehydration and char formation at high temperatures, forming a stable char layer that effectively blocks oxygen and heat transfer to the interior

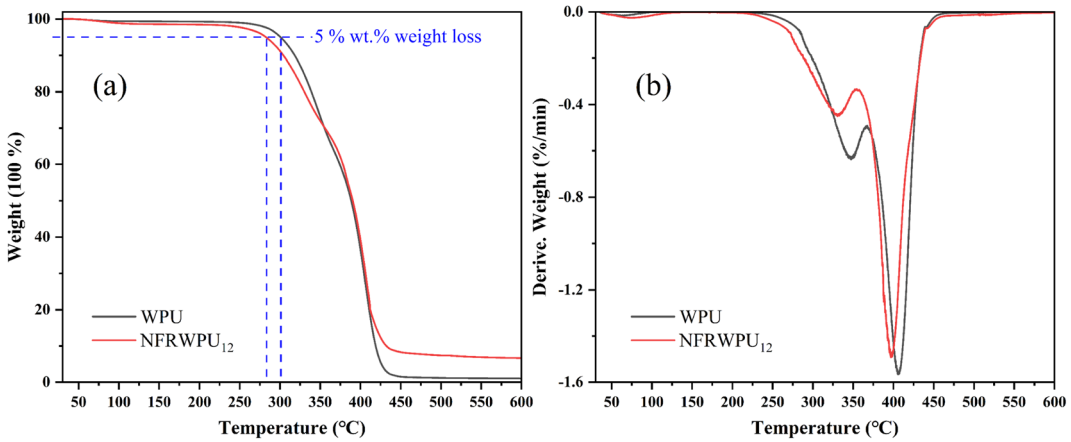

Fig. 4 (a) TGA and (b) DTG curves of WPU and $NFRWPU_{12}$ in N_2 atmosphere.

Table 4 Thermogravimetric data of WPU and $NFRWPU_{12}$[a]

Sample	$T_{5\%}$ (°C)	T_{max_1} (°C)	T_{max_2} (°C)	RT_{max_1} (% min^{-1})	RT_{max_2} (% min^{-1})	Carbon residue (%)
WPU	301.72	347.65	406.25	−0.63	−1.56	0.92
$NFRWPU_{12}$	283.63	331.32	397.41	−0.44	−1.49	6.55

[a] $T_{5\%}$ denotes the temperature at 5 wt% weight loss, taken as the onset degradation temperature. T_{max} denotes the temperature of the maximum mass loss rate (the DTG peak maximum). RT_{max} denotes the maximum weight loss rate.

Table 5 LOI and vertical burning test results of NFRWPU

Sample	LOI (%)	Ignition the filter paper	Dripping	Self-extinguish time after leaving the fire (s)
WPU	18.5	Yes	Yes	18
$NFRWPU_9$	21.4	Yes	Yes	13
$NFRWPU_{12}$	25.6	No	No	5
$NFRWPU_{15}$	23.3	No	No	7

material, thereby preventing further material combustion. Additionally, phosphorus-containing gases released by PHAD during combustion can capture combustion radicals in the gas phase, suppress combustion chain reactions, and reduce flame spread rate and intensity.[13] These results consistent with TGA test results. Interestingly, with the gradual increase in PHAD content, the LOI value of NFRWPU film shows an initial increase followed by a decrease trend. The reason might be that higher phosphorus content in NFRWPU structure resulted in a lower thermal decomposition temperature, causing the molecular chains to crack easier and produce more flammable gases at the ignition temperature.[29]

Fig. 5 shows the digital images of vertical burning tests for NFRWPU films. It can be observed that films containing PHAD has better thermal stability at high temperatures compared to pure WPU. When WPU is ignited, burning molten derivatives continue to fall and ignite the filter paper below. In contrast, the flame retardancy of NFRWPU is significantly improved without any droplets igniting the filter paper. As shown in Fig. 5b–d, the self-extinguish time after leaving fire in vertical burning tests are 13, 5 and 7 seconds, respectively. These results showed that the NFRWPUs can effectively suppress melt dripping during combustion, greatly raise the LOI value (25.6% for $NFRWPU_{12}$), self-extinguishes within 5 s after leaving the fire, and the filter paper below the sample does not ignite. This could be due to the poor thermal stability of the P–O–C bonds on the NFRWPU molecular chains, which easily decompose under heat, causing the flame-retardant groups to break off before they can effectively act, thus reducing the flame-retardant effect.

Char residues surface analysis

In Fig. 6, the morphologies and element analysis of the char residues after vertical burning test were investigated by SEM and EDS, respectively. It has been reported that the physical structure of the charring layer plays a very important role in preventing heat transfer, flame spread, and droplet generation during the combustion process.[25] The WPU is easily ignitable

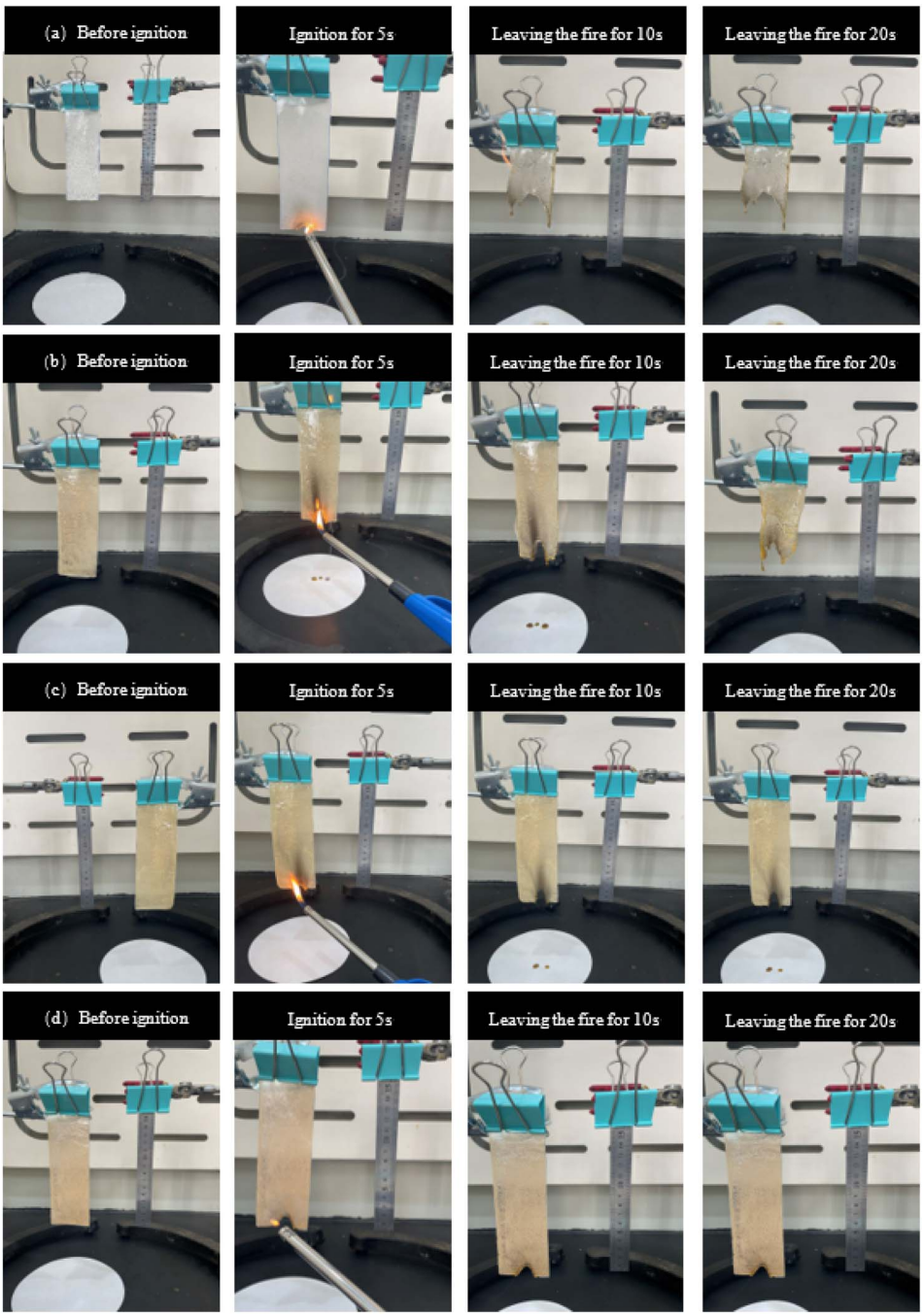

Fig. 5 Digital images of vertical burning test of (a) WPU, (b) $NFRWPU_9$, (c) $NFRWPU_{12}$ (d) $NFRWPU_{15}$.

and highly flammable material due to its cellular structure, low heat capacity, low thermal conductivity and high internal surface area. In Fig. 6a, SEM analysis reveals that the untreated WPU exhibits loose, thin, blocky char residues with numerous pores and some cracks, indicative of its flammability. In contrast, in Fig. 6b, $NFRWPU_{12}$ shows a more continuous, dense, and thicker layered structure. This continuous char layer can act as a protective shield to prevent heat transfer, oxygen diffusion and flammable gases release, suggesting suppression during combustion. The main causes of these are the carbonization of the aromatic framework, the matrix, and the char-forming action of phosphorus-containing groups. Elemental analysis showed that the char residues of $NFRWPU_{12}$ film contained P elements, which confirmed the successful synthesis of NFRWPU emulsion. As shown in Fig. 6c, there are only C, N, O elements in WPU residual char. However, in Fig. 6d, for $NFWPU_{12}$, there are 17.86 wt% P elements besides C and O element. This confirmed that PHAD was incorporated into $NFRWPU_{12}$. The P and O elements were present in the form of polyphosphates, which played a catalytic and dehydrating part in promoting formation of char layers in condensed phase,

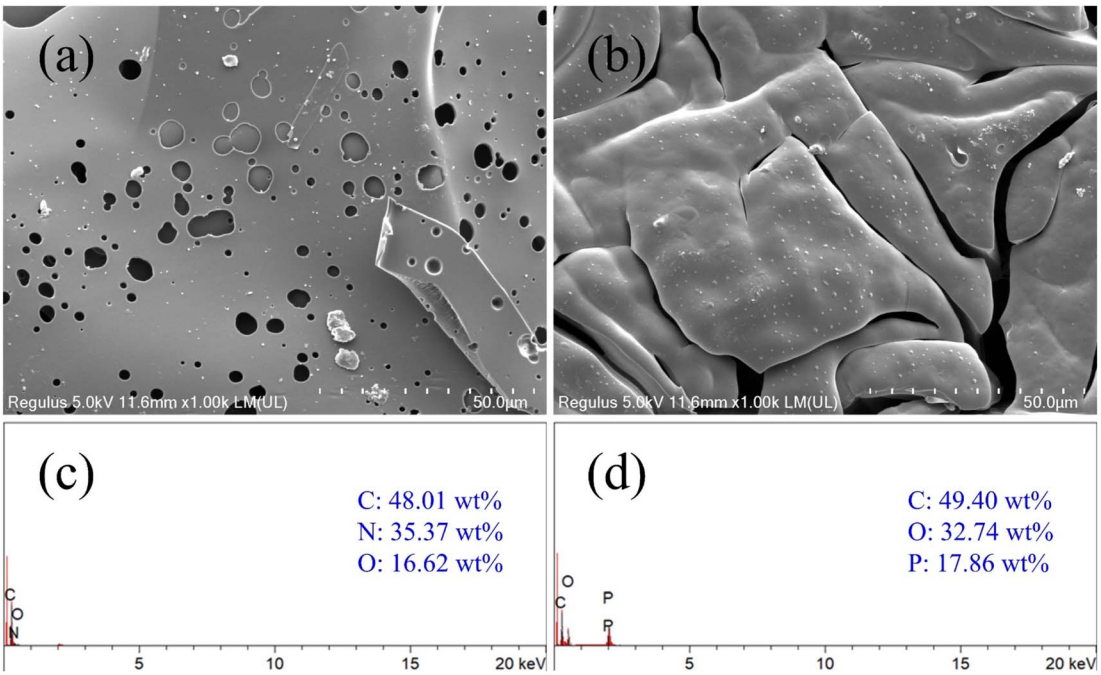

Fig. 6 SEM micrographs images of carbon residue (a) WPU, (b) $NFRWPU_{12}$; EDS spectra of the char residue (c) WPU, (d) $NFRWPU_{12}$.

protecting the polymer matrix by preventing the transfer of oxygen, combustible gases, and heat from combustion zone.

Conclusions

A phosphorus-containing DOPO-based Schiff base derivative (PHAD) was synthesized as a flame-retardant monomer and incorporated into WPU molecular chain as a chain extender, thereby synthesizing a series of NFRWPU materials. The chemical structures were characterized by FT-IR and NMR. Some key performance of NFRWPU in application were investigated, including:

(1) Physical properties were characterized including appearance, storage stability, viscosity and particle size. With the increase of PHAD content, the appearance of the emulsion gradually become darker; when PHAD content reaches 15%, the emulsion can pass stability test. Both the particle size and viscosity of the emulsion increase gradually with increasing PHAD content. The average particle size of pure WPU is 49.3 nm with a viscosity of 67 mPa s. When the PHAD content reaches 12%, the average particle size of emulsion increases to 106.6 nm with a viscosity of 89 mPa s.

(2) Mechanical properties were characterized including tensile strength and elongation at break. With the increase of PHAD content, tensile strength of NFRWPU initially increases and then decreases, while elongation at break decreases continuously. Pure WPU exhibits a high elongation at break of 1380% with tensile strength only 2.83 MPa. When the PHAD content increases from 9% to 12%, the tensile strength of the film significantly increases from 10.61 MPa to 22.63 MPa. However, further increase the PHAD content leads to a decrease in tensile strength to 13.08 MPa.

(3) Thermal stability of NFRWPU was also influenced by the PHAD content. Adding PHAD reduces $T_{5\%}$, T_{max} and RT_{max} of the film while increasing the carbon residue. As the PHAD content increases from 0 to 12%, the $T_{5\%}$ of WPU films decreases from 301.72 °C to 283.63 °C for $NFRWPU_{12}$ films, and the carbon residue increases from 0.92% to 6.55%.

(4) Flammability analysis. The flame retardancy of NFRWPU films increased significantly with the increase of PHAD content. Specifically, as PHAD content increases from 0 to 15%, the LOI value of the film first increases from 18.5% to 25.6% and then decreases to 23.3%. The flame retardancy mechanism was verified by residual carbon characterization (SEM and EDS). All of the results implied that NFRWPU would be a promising flame retardant WPU, furthermore, considering the comprehensive performance, the optimal PHAD content is determined to be 12%.

Data availability

Data for this article are available at **https://github.com/wwm0909501/non-ionic-flame-retardant-waterborne-polyurethane**.

Author contributions

Hongping Tong: data curation, visualization, conceptualization, writing – original draft preparation. Wang Weimin: writing – reviewing and editing, investigation. Gui Wang: project administration. Xiaojun Wang: resources. Dongmei Yu: investigation. Bajin Chen: resources. Kemei Pei: supervision.

Conflicts of interest

There are no conflicts to declare.

Acknowledgements

The author(s) disclosed receipt of the following financial support for the research, authorship, and/or publication of this article: this study was financially supported by the Key R&D Program of Zhejiang Province (2024C01186).

Notes and references

1 L.-P. Zhang, Z.-G. Zhao, Y.-Y. Huang, C.-J. Zhu, X. Cao and Y.-P. Ni, *Polymers*, 2023, **15**, 2400.
2 R. K. Gupta and A. K. Mishra, *Eco-friendly Waterborne Polyurethanes: Synthesis, Properties, and Applications*, CRC Press, 2022.
3 L. Liu and R. Lv, *e-Polym.*, 2019, **19**, 235–243.
4 H. Wang, X. Du, S. Wang, Z. Du, H. Wang and X. Cheng, *RSC Adv.*, 2020, **10**, 12078–12088.
5 X. Yin, Y. Luo and J. Zhang, *Ind. Eng. Chem. Res.*, 2017, **56**, 1791–1802.
6 J. Zhou, T. Zhang, Y. Xu and X. Zhang, *Prog. Org. Coat.*, 2023, **182**, 107631.
7 X. Qian, Q. Liu, L. Zhang, H. Li, J. Liu and S. Yan, *Polym. Degrad. Stab.*, 2022, **197**, 109852.
8 S. Lu, Y. Feng, P. Zhang, W. Hong, Y. Chen, H. Fan, D. Yu and X. Chen, *Polymers*, 2021, **13**, 1730.
9 Y. Sun, C. Liu, Y. Hong, R. Liu and X. Zhou, *Prog. Org. Coat.*, 2019, **137**, 105323.
10 P. Zhang, S. Tian, H. Fan, Y. Chen and J. Yan, *Prog. Org. Coat.*, 2015, **89**, 170–180.
11 L. Feng, W. Wang, B. Song, X. Zhu, L. Wang, R. Shao, T. Li, X. Pei, L. Wang and X. Qian, *Prog. Org. Coat.*, 2023, **174**, 107286.
12 Z.-J. Cao, X. Dong, T. Fu, S.-B. Deng, W. Liao and Y.-Z. Wang, *Polym. Degrad. Stab.*, 2017, **136**, 103–111.
13 H. Wang, S. Wang, X. Du, Z. Du, H. Wang and X. Cheng, *J. Appl. Polym. Sci.*, 2020, **137**, 49368.
14 A. M. Szczotok, D. Madsen, A. Serrano, M. Carmona, P. Van Hees, J. F. Rodriguez and A.-L. Kjøniksen, *J. Mater. Sci.*, 2021, **56**, 1172–1188.
15 T. Guler, U. Tayfun, E. Bayramli and M. Dogan, *Thermochim. Acta*, 2017, **647**, 70–80.
16 X. Liang, C. Liu, Y. Chen, F. Yin, D. Bao and G. Zhou, *Prog. Org. Coat.*, 2023, **177**, 107388.
17 M.-J. Xu, G.-R. Xu, Y. Leng and B. Li, *Polym. Degrad. Stab.*, 2016, **123**, 105–114.
18 Y. Ren, Y. Dong, Y. Zhu, J. Xu and Y. Yao, *Prog. Org. Coat.*, 2019, **129**, 309–317.
19 Y. Qiao and X.-d. Zhang, *J. Electron. Res. Appl.*, 2024, **8**, 84–92.
20 Q. Feng, G. Chen and J. Liang, *Modell., Meas. Control, C*, 2018, **79**, 222–228.
21 Y. Yin, M. Feng, J. Yao and J. Niu, *J. Wuhan Univ. Technol., Mater. Sci. Ed.*, 2024, **39**, 497–505.
22 S. Ghosh, S. Ganguly, S. Remanan, S. Mondal, S. Jana, P. K. Maji, N. Singha and N. C. Das, *J. Mater. Sci.: Mater. Electron.*, 2018, **29**, 10177–10189.
23 L. Wu, J. Guo and S. Zhao, *Polym. Bull.*, 2017, **74**, 2099–2116.
24 Z. Zhao, D.-M. Guo, T. Fu, X.-L. Wang and Y.-Z. Wang, *Polymer*, 2020, **205**, 122780.
25 M. Cui, J. Li, X. Chen, W. Hong, Y. Chen, J. Xiang, J. Yan and H. Fan, *Prog. Org. Coat.*, 2021, **158**, 106359.
26 S. Gaan, S. Liang, H. Mispreuve, H. Perler, R. Naescher and M. Neisius, *Polym. Degrad. Stab.*, 2015, **113**, 180–188.
27 M. Zhang, Z. Luo, J. Zhang, S. Chen and Y. Zhou, *Polym. Degrad. Stab.*, 2015, **120**, 427–434.
28 H. Wang, S. Wang, X. Du, H. Wang, X. Cheng and Z. Du, *RSC Adv.*, 2019, **9**, 7411–7419.
29 Y. Yin, M. Feng, W. Li, J. Yao and J. Niu, *J. Appl. Polym. Sci.*, 2023, **140**, e54674.